ADVANCED MATERIALS
www.advmat.de

www.MaterialsViews.com

A Fiber Supercapacitor with High Energy Density Based on Hollow Graphene/Conducting Polymer Fiber Electrode

Guoxing Qu, Jianli Cheng, Xiaodong Li, Demao Yuan, Peining Chen, Xuli Chen, Bin Wang,* and Huisheng Peng**

Wearable electronics are becoming part of our lives and present attractive prospects for smart skins,[1] interfacing computers/processors,[2] and stretchable circuitries.[3] To power these wearable electronic devices, flexible power sources are needed. Among various flexible power sources, fiber-shaped supercapacitors have attracted increasing attention due to their merits of low weight, tiny volume, high flexibility, and wearability.[4] Unlike conventional rigid planar supercapacitors, 1D fiber-shaped supercapacitors can be directly used as flexible power sources in wearable textile/fabric electronics.[5] However, compared with batteries or traditional planar supercapacitors, fiber supercapacitors show much lower energy densities and suffer from a great challenge in mechanical performance. It is well known that the energy of the supercapacitor is proportional to its capacitance in a specific voltage window. Meanwhile, the capacitance is highly dependent on the intrinsic charge storage capabilities of electrode materials. Therefore, increasing interest is attracted to explore fiber supercapacitors with both high specific capacitance and mechanical property.

Recently, significant achievements have been made through the use of carbon-based fibers that were prepared from carbon nanotube (CNT),[6] reduced graphene oxide (RGO),[7] and activated carbon[8] as well as their composites with conducting polymers such as polyaniline,[9,10] and poly(3,4-ethylenedioxythiophene),[11,12] and pseudocapacitive inorganic moieties.[13–15] For instance, two CNT/polyaniline composite yarns were twisted into a supercapacitor with a specific capacitance of 38 mF cm^{-2} at 0.01 mA cm^{-2};[16] two CNT/Co_3O_4 composite yarns were also twisted to fabricate a fiber supercapacitor to display a specific capacitance of 52.6 mF cm^{-2} at 0.053 mA cm^{-2};[17] polyelectrolyte-wrapped graphene/CNT core-sheath fibers had been made into supercapacitors with a specific capacitance of 177 mF cm^{-2} at 0.1 mA cm^{-2}.[4]

Although the capacitance and energy density of the fiber supercapacitor have been largely improved, it is still too low to meet the requirements of practical applications in electronics. A lot of efforts are needed to develop general and effective strategies to further enhance them. It is well known that an electric double-layer capacitor stores charges through a surface double-layer capacitance mechanism of active materials and separates the charges at the electrode/electrolyte interface.[10,18] Therefore, an increase in interfacial area will greatly promote the specific capacitance and energy density. However, the available fiber electrodes are solid, and only their outer surfaces can be used to effectively interact with the electrolyte with low interfacial areas.[19] It is expected that, if a fiber electrode is hollow, the additional inner interface of the fiber electrode would contribute much more specific capacitance to the fiber supercapacitor. In other words, a larger interior hollow part in the fiber would produce a higher specific surface area, thus bringing higher electrode/electrolyte contact interface and facilitating transport of charges.

Here, hollow fiber electrodes including hollow RGO/conducting polymer composite fibers (labeled as HCFs) and hollow bare RGO fibers (labelled as HPFs) are created with high flexibility and electrical conductivity. They can be tied into knots, rolled up and woven into textiles. The electrical conductivities of the HCFs and HPFs reach 4700 and 4200 S m^{-1} even without taking the hollow interior into account, respectively. Symmetric fiber supercapacitors based on two parallel HCF electrodes and poly(vinyl alcohol) PVA/H_3PO_4 gel electrolyte show an extremely high charge-storage capability and a high resistance to bending fatigue. The HCF fiber supercapacitor demonstrates specific areal capacitances up to 304.5 mF cm^{-2} (or 143.3 F cm^{-3} or 63.1 F g^{-1}) at 0.08 mA cm^{-2}, which corresponds to an ultra-high energy density of 27.1 μW h cm^{-2} at a power density of 66.5 μW cm^{-2}. To the best of our knowledge, they represent the highest areal capacitance and areal energy density in fiber supercapacitors to date. In addition, the specific capacitance remains almost unchanged after bending for 500 times and can be maintained by 96% after 10 000 cycles.

The preparation of an HCF is schematically shown in **Figure 1**a. A mixture of a solution of graphene oxide (GO), poly(3,4-ethylenedioxythiophene):poly(styrenesulfonate) (PEDOT:PSS), and vitamin C (VC) is injected into a glass pipe, followed by sealing the two ends of the pipe to reduce GO to RGO in the mold pipe. The two ends are then opened to further dry and reduce the wet fiber to synthesize the HCF. The HPF has been prepared through the same procedure but without the addition of PEDOT:PSS.

The hollow fibers were first analyzed by scanning electron microscopy (SEM). Figure 1b shows a typical cross-sectional SEM image of RGO composite fiber with an obvious interior hole. The RGO sheets are nematic and aligned along the length

G. Qu, Prof. J. Cheng, Dr. X. Li, D. Yuan, Prof. B. Wang
Institute of Chemical Materials
China Academy of Engineering Physics
Mianyang, Sichuan 621900, China
E-mail: jianlicheng@caep.cn; binwang@caep.cn
Prof. J. Cheng, P. Chen, Dr. X. Chen, Prof. H. Peng
State Key Laboratory of Molecular Engineering of Polymers
Department of Macromolecular Science
and Laboratory of Advanced Materials
Fudan University
Shanghai 200438, China
E-mail: penghs@fudan.edu.cn

DOI: 10.1002/adma.201600689

© 2016 WILEY-VCH Verlag GmbH & Co. KGaA, Weinheim

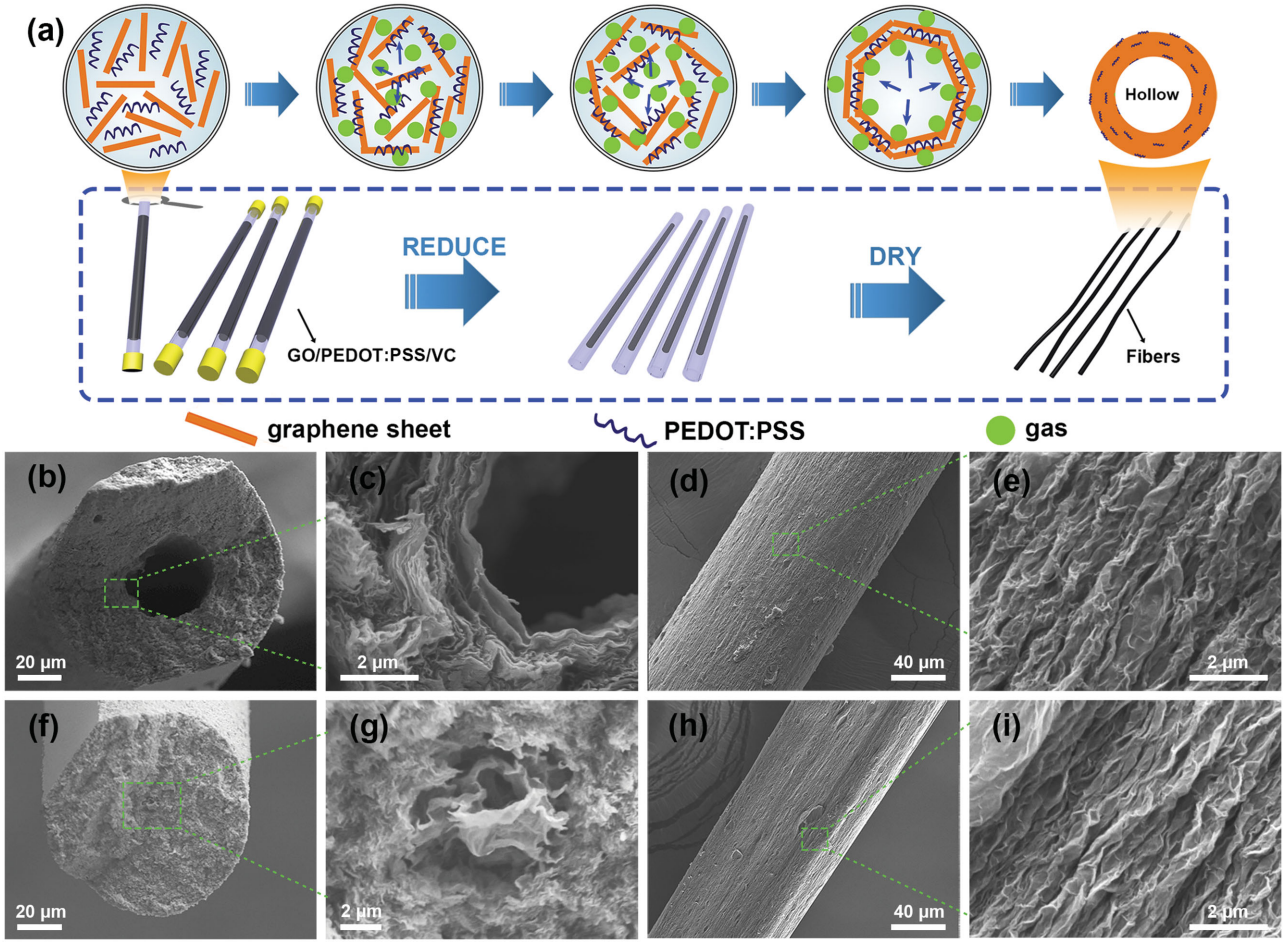

Figure 1. Preparation of HCFs and formation of hollow structures. a) Schematic illustration. b,c) Cross-sectional SEM images of the HCF at low and high magnifications, respectively. d,e) SEM images of the HCF by a side view at low and high magnifications, respectively. f,g) Cross-sectional SEM images of the HPF at low and high magnifications, respectively. h,i) SEM images of the HPF by a side view at low and high magnifications, respectively.

of the composite fiber (Figure 1c). The HCF was rough and wrinkled on the surface (Figure 1d,e), which increased specific areas of electric double layers for the supercapacitors. The ratios of the inner to the outer diameters were gradually increased with the increasing polymer weight percentage from 10% to 33% in the composite fibers (Figure S1, Supporting Information). For a bare RGO fiber, a much smaller hollow part was observed at the center (Figure 1f,g), and it shared a wrinkled surface (Figure 1h,i). Note that the reduction process should be made in a closed reactor. If the two ends of the glass pipe were not fastened up during the preparation, both bare and composite RGO fibers were produced to be solid (Figure S2, Supporting Information).

The appearance of the hollow structure might be derived from the released gases during the reduction reaction of GO and summarized below. When the mold pipe is tightly sealed, there exists a pressure difference between the solution interior and the void space at the two ends of the pipe. Gases such as carbon dioxide originated from the reduction of the functional groups on GO are released from the solution interior and thus a subminiature airflow will be formed from the solution interior to the void space. Therefore, the formed RGO sheets in the center will be pushed away from the axis by the airflow (Figure 1a). The accumulated gases in the void space were verified by the supporting video. When PEDOT:PSS is added to the GO solution, GO can easily form lyotropic nematic liquid crystals,[20] and the hydrophilic function groups in PSS facilitate the diffusion of RGO sheets to promote the formation of hollow structure. Therefore, the diameters of hollow parts in the composite fibers are much larger than those in the bare RGO fibers.

The HCF was flexible and could be tied into a knot without obvious damage in structure (**Figure 2**a,b). The hollow structure was favorable for resisting the outer stress with both high flexibility and stability. For instance, the hollow fibers could be transformed into belts instead of cracking under twisting (Figure 2c). As expected, the HCFs could be woven into flexible textiles with the other fibers such as cotton fibers (Figure 2d,e). The hollow composite fiber may be continuously prepared and wrapped on a cardboard tube for a large-scale production (Figure 2f). The HCF exhibited a tensile strength up to 631 MPa (Figure S3a, Supporting Information) and could lift up objects above 120 g (Figure 2g), which was thousand times heavier than that of the HCF. The high tensile strength may

© 2016 WILEY-VCH Verlag GmbH & Co. KGaA, Weinheim

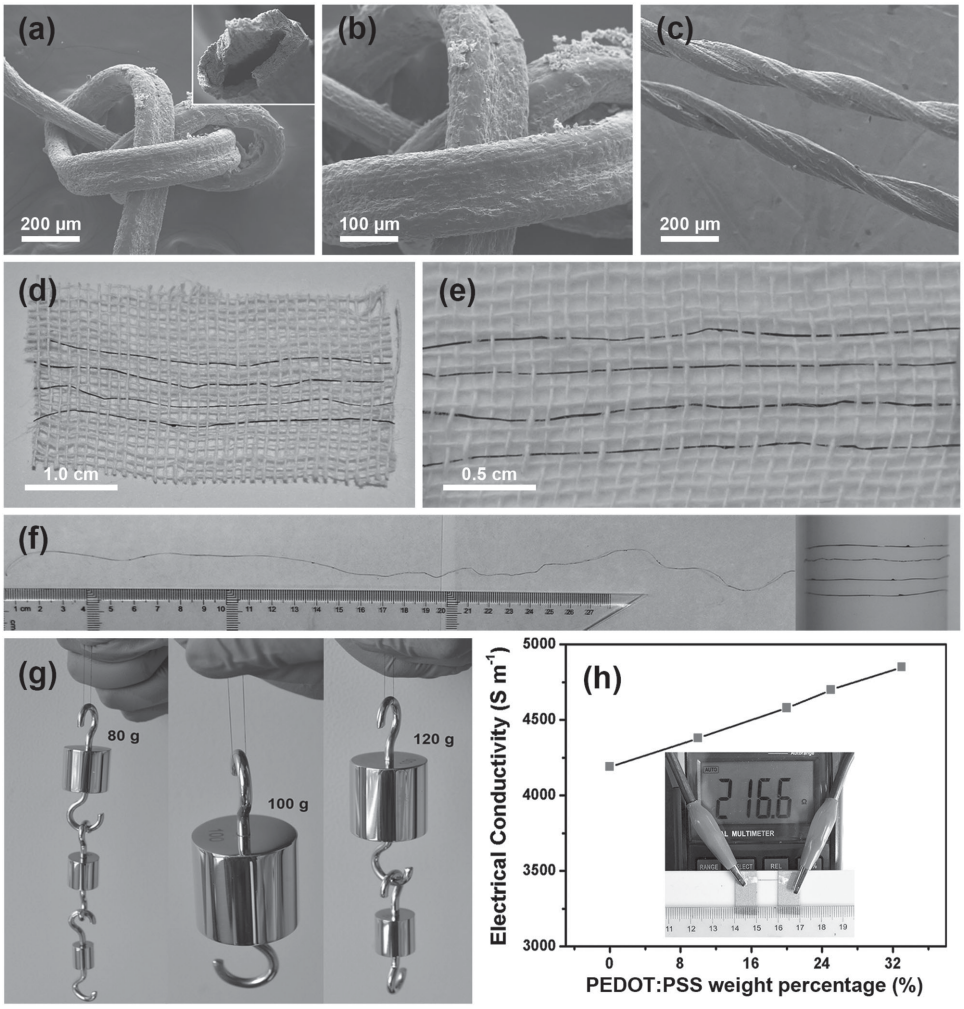

Figure 2. Mechanical and electronic properties of HCFs. a,b) SEM images of a knotted fiber at low and high magnifications, respectively. The inset in (a) is a cross-sectional SEM image of the knotted fiber. c) SEM image of two twisted HCFs. d,e) Photographs of HCFs being woven with cotton fibers at low and high magnifications, respectively. f) Photograph of a long hollow HCF wrapped on a cardboard tube. g) An HCF being loaded with objects with increasing weights. h) Dependence of electrical conductivity on PEDOT:PSS weight percentage. The inserted photograph shows an electrical resistance of 216.6 Ω with a length of 1 cm and outer diameter of 112 μm.

be attributed to nematic RGO sheets with aligned structure along the length of the composite fiber, π–π interactions among the reduced GO sheets and effective integration of RGO and PEDOT. These hollow fibers were electrically conductive, and the conductivities were approximately linearly increased with the increasing polymer weight percentage (Figure 2h), e.g., 4200 S m^{-1} for a bare RGO fiber, and 4700 S m^{-1} for a composite fiber at a polymer weight percentage of 25%.

To investigate the electrochemical performances of the hollow fiber electrodes, symmetric solid-state fiber supercapacitors were fabricated using a PVA/H_3PO_4 gel electrolyte. Here a high-performance fiber supercapacitor was made from two parallel fiber electrodes (Figure S4, Supporting Information). Cyclic voltammetry (CV) curves based on the RGO composite fibers with increasing polymer weight percentages were compared in Figure S3b (Supporting Information). The weight percentage at 25% displayed the best capacitive behavior and would be discussed below.

CV curves of the fiber supercapacitors based on HPFs and HCFs with the increasing scan rates from 5 to 100 mV s^{-1} are shown in Figure S5a,c (Supporting Information), respectively. A rectangular shape profile was shared for both HPF and HCF, indicating a typical behavior of electrochemical double layer capacitor.[21] Compared with the HPF, the CV curves for the HCF can better retain a rectangular shape even at a high scan rate of 100 mV s^{-1}, which revealed a more rapid charge transport and higher rate performance. Note that although the CV curves based on the HPF were slightly deformed with the increasing scan rates due to a relatively low electrical conductivity, a higher capacitive behavior was observed in comparison with the previous reports from the RGO.[22] Figure S5b,d (Supporting Information) shows the galvanostatic charge-discharge profiles for the HPF and HCF at current densities of 0.08, 0.25, 0.5, 0.75, and 1.0 mA cm^{-2}, respectively. All of them shared a typical triangular shape that demonstrated a rapid charge transport between the two fiber electrodes. The linear

© 2016 WILEY-VCH Verlag GmbH & Co. KGaA, Weinheim

relationship between potential and time also verified the electric double layer capacitance behavior. The symmetry between charge and discharge curves indicates a Coulombic efficiency of ≈100%, revealing a high reversibility of the device and good charge propagation between the two electrodes. No obvious voltage drops were found until the current density rose to 0.75 mA cm^{-2} for the HCF; for the HPF, obvious voltage drops occurred at no more than 0.5 mA cm^{-2}, which agreed with the deformed CV curves at a high scan rate.

At a relatively low scan rate or current density, the resistance of fiber electrode shows a relatively lower impact on the capacitance, which favors the study on the capacitive properties of hollow fibers. To separately investigate the contribution of the hollow part to the capacitance, the CV curves were compared at a low scan rate of 20 mV s^{-1} and galvanostatic charge–discharge profiles were compared at a low current density of 0.08 mA cm^{-2} for the hollow and solid fibers with the same length. The area of the rectangular curve for the hollow fiber, particularly the HCF, was much larger than the solid counterpart, indicating that the hollow fiber did display a better charge-storage capability as an electrode (Figure S5e, Supporting Information). The discharge time for the HCF, HPF, solid RGO composite fiber, and solid bare RGO fiber had been obtained as 1466, 991, 910, and 919 s at 0.08 mA cm^{-2}, respectively (Figure S5f, Supporting Information). Therefore, the HCF showed a higher capacitance than both HPF and solid fiber electrodes.

For fiber supercapacitors, the mass of the fiber electrode was typically low, and the limited space remained a key constraint.[23] Therefore, the specific capacitance, and energy and power densities based on area or volume are more useful for evaluation.[24] The HCF-based supercapacitor revealed an ultra-high specific areal capacitance of 304.5 mF cm^{-2} (143.3 F cm^{-3} or 63.1 F g^{-1}) at 0.08 mA cm^{-2} (**Figure 3**a), which was about six times of the CNT@Co_3O_4 fibers[17] and CNT@PANI fibers.[16] The corresponding length capacitance was 8.1 mF cm^{-1}. Figure 3b shows the electrochemical impedance spectroscopy (EIS) of the HCF and HPF-based supercapacitors. In the high-frequency region, the X-intercept of the Nyquist plot represents the equivalent series resistance (ESR) that corresponds to the electrolyte resistance, the internal resistance of the electrode and the contact resistance.[25] We fitted the EIS data based on an equivalent circuit model (Figure S5g, Supporting Information). According to the fitting results, ESR of HCF-based supercapacitor is 306.8 Ω, much lower than that of HPF-based supercapacitor (605.4 Ω). This result may be attributed to high conductivity and large surface area of the HCF with larger accessible electrode/electrolyte interface. The specific surface areas of HCFs and HPFs were measured as 71.0 and 40.6 m^2 g^{-1}, respectively (Figure S6a, Supporting Information). The ESR values are lower than those based on single-walled CNTs, an ideal electrode material for wearable electronics.[26] In the low-frequency region, the verticality of the sloped line showed their capacitive behavior. The sloped lines for HCFs are more close to the theoretical vertical line compared with that of HPFs and show characteristic features of pure capacitive behavior, indicating faster ion diffusion behavior.[17] Furthermore, the projected length of the sloped line on the real impedance axis can be used to characterize the ion penetration process.[27] The curve length of HCF was shorter than that of the HPF, indicating that the HCF had a faster ion diffusion[28] and thus confirming the improved kinetics due to the large hollow interior in HCF. These results revealed that high conductivity and good ion diffusion behavior of the HCFs are beneficial to a better performance of fiber electrode.

Figure 3c shows Ragone plots based on the entire supercapacitor. For both hollow fibers, the curves were relatively flat, indicating that the high energy density of the fiber supercapacitors had been maintained during the increasing power output. The fiber supercapacitors based on HCFs showed an excellent charge storage capability with an ultra-high areal energy density of 27.1 μW h cm^{-2} (based on a fiber electrode) or 6.8 μW h cm^{-2} (based on the entire device) at a power density of 66.5 μW cm^{-2} or 16.6 μW cm^{-2}. The volumetric energy density based on one fiber electrode was 12.7 mW h cm^{-3} (Figure S6b, Supporting Information), which was 4 to 6 times those of the other fiber supercapacitors (2.16–3.4 mW h cm^{-3}).[29,30] The volumetric energy density based on the entire device was 3.2 mW h cm^{-3}, which was even similar to that of 4 V–500 μAh thin-film lithium batteries (0.3–10 mW h cm^{-3}) and higher than those of planar supercapacitors (3.1 mW h cm^{-3}).[31] Two 2.6-cm-long fiber supercapacitors connected in series can power a light emitting diode (LED) for 5 min (inset in Figure 3c). Previously, more fiber supercapacitors were required to power such an LED that was operated at a minimum voltage of 1.7 V because the voltage of low energy density supercapacitors dropped rapidly.

The cyclic stability of the fiber supercapacitor was investigated by galvanostatic charge–discharge test (Figure 3d). Both HCF and HPF-based supercapacitors showed a high cyclic stability. For the HCFs-based supercapacitor, the specific capacitance was maintained by 96% after more than 10 000 cycles. As shown in Figure S7a (Supporting Information), the capacitance decay is negligible even after soaking the HCFs in gel electrolyte for 60 d. Meanwhile, by comparing the fourier transform infrared spectroscopy spectra of the gel electrolyte before and after cycling for 1000 cycles, the characteristic peaks of the sulfonic acid group of the PSS chain could not be observed at the range of 1200–1000 cm^{-1} (in Figure S7b, Supporting Information), further revealing the high stability of the electrode in gel electrolyte. The connected fiber supercapacitors in serial could be pasted on clothes as a wearable power source to light up three LEDs (inset in Figure 3d).

Figure 3e further compares the electrochemical performance of fiber supercapacitors. To our best knowledge, this HCF-based fiber supercapacitor displayed the highest specific capacitance. Even the volume of the hollow interior was not excluded when calculating the volumetric capacitance, this fiber supercapacitor produced a high volumetric capacitance of 143.3 F cm^{-3}. For the HPF, a high areal capacitance of 212.9 mF cm^{-2} (6.0 mF cm^{-1}, 94.6 F cm^{-3}, or 60.0 F g^{-1}) had been also achieved. In contrast, the areal capacitances for the solid composite and bare RGO fibers were much lower, i.e., 189.2 mF cm^{-2} (67.0 F cm^{-3} or 50.8 F g^{-1}) and 186.8 mF cm^{-2} (79.9 F cm^{-3} or 43.1 F g^{-1}), respectively. Accordingly, the capacitances of HPFs and HCFs were increased by 12% and 60% due to the design of a hollow interior and the incremental mechanism is detailed below.

© 2016 WILEY-VCH Verlag GmbH & Co. KGaA, Weinheim

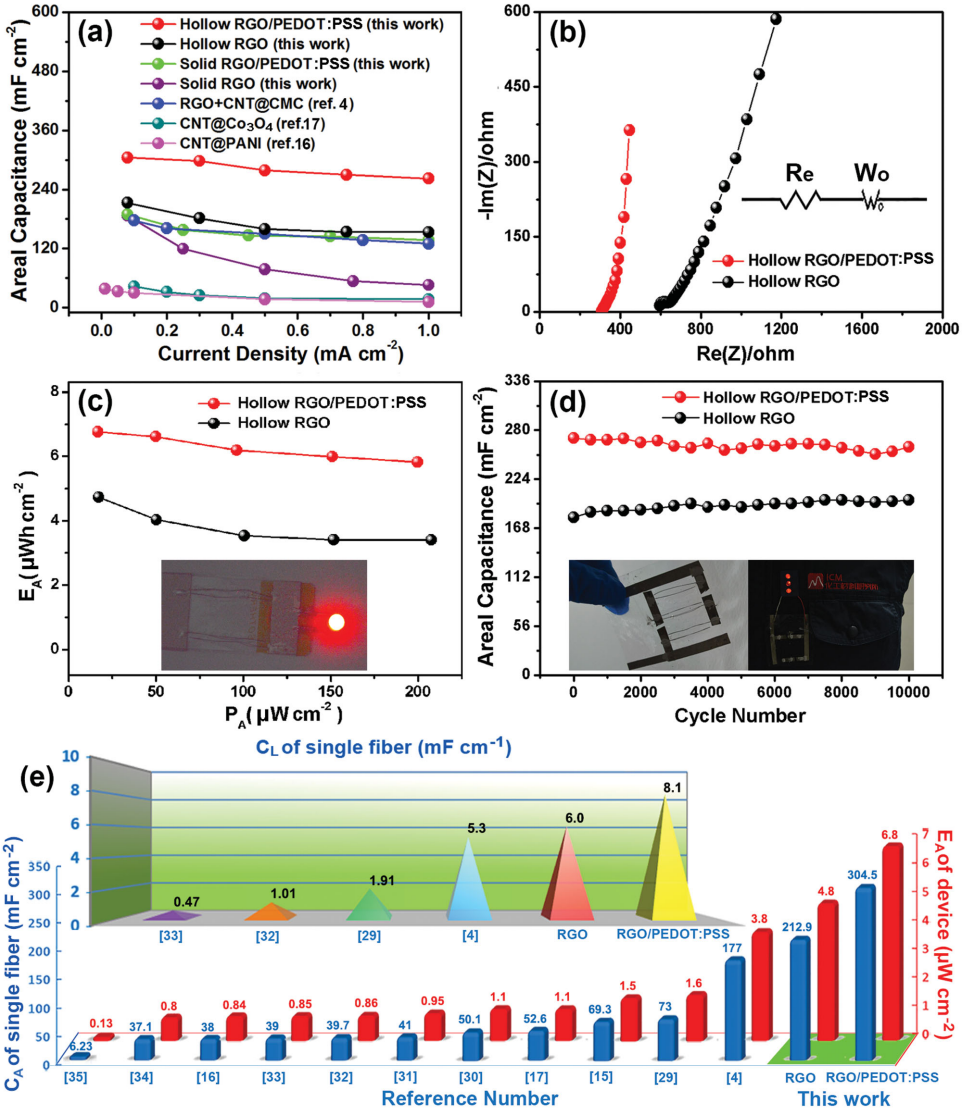

Figure 3. Electrochemical performances of the fiber supercapacitors based on HCFs and HPFs. a) Areal specific capacitances at increasing current densities. b) Electrochemical impedance spectra with increasing frequencies from 50 kHz to 100 mHz. c) Ragone plots based on the entire fiber supercapacitor. The inserted photograph shows that a serial fiber supercapacitor lights up a red LED. d) Long-term cyclic stability of the fiber supercapacitors based on HCFs and HPFs at 0.48 mA cm^{-2}. The inserted photograph displays that three fiber supercapacitors are connected in serial and pasted onto clothes to power three LEDs. e) Comparison of the electrochemical performances of HCF-based fiber supercapacitors with the other fiber-shaped supercapacitors in areal specific capacitance (C_A), length specific capacitance (C_L), and areal energy density (E_A).

For an electrical double layer capacitor (**Figure 4**a), the specific capacitance is proportional to the face-to-face area of the two parallel-plates.[32] Thus, the capacitance (C) of a fiber supercapacitor is approximately calculated from Equation (1)

$$C = \frac{\varepsilon S}{4\pi kd} = KS \tag{1}$$

Here ε, π, k, and d represent the fundamental constants in parallel-plate capacitor, K is an integrated constant, and S is the face-to-face area in parallel-plate capacitors and corresponds to the area of the electrode/electrolyte interface in fiber supercapacitor. The change rate of the capacitance (R_C) should be theoretically equal to the superficial area change rate (R_A) of the fiber and could be obtained from Equation (2)

$$R_C = R_A = \frac{\pi L d_{in}}{\pi L d_{ou}} = \frac{d_{in}}{d_{ou}} \tag{2}$$

Here d_{in}, d_{ou}, and L are the inner diameter, outer diameter, and effective length of hollow fiber electrode, respectively. According to the diameter ratio mentioned above, the R_A values of HPF and HCF are 11% and 58%, which agree with the R_C values of the resulting fiber supercapacitors (12% and 60%), respectively. The agreement between R_A and R_C demonstrates

© 2016 WILEY-VCH Verlag GmbH & Co. KGaA, Weinheim

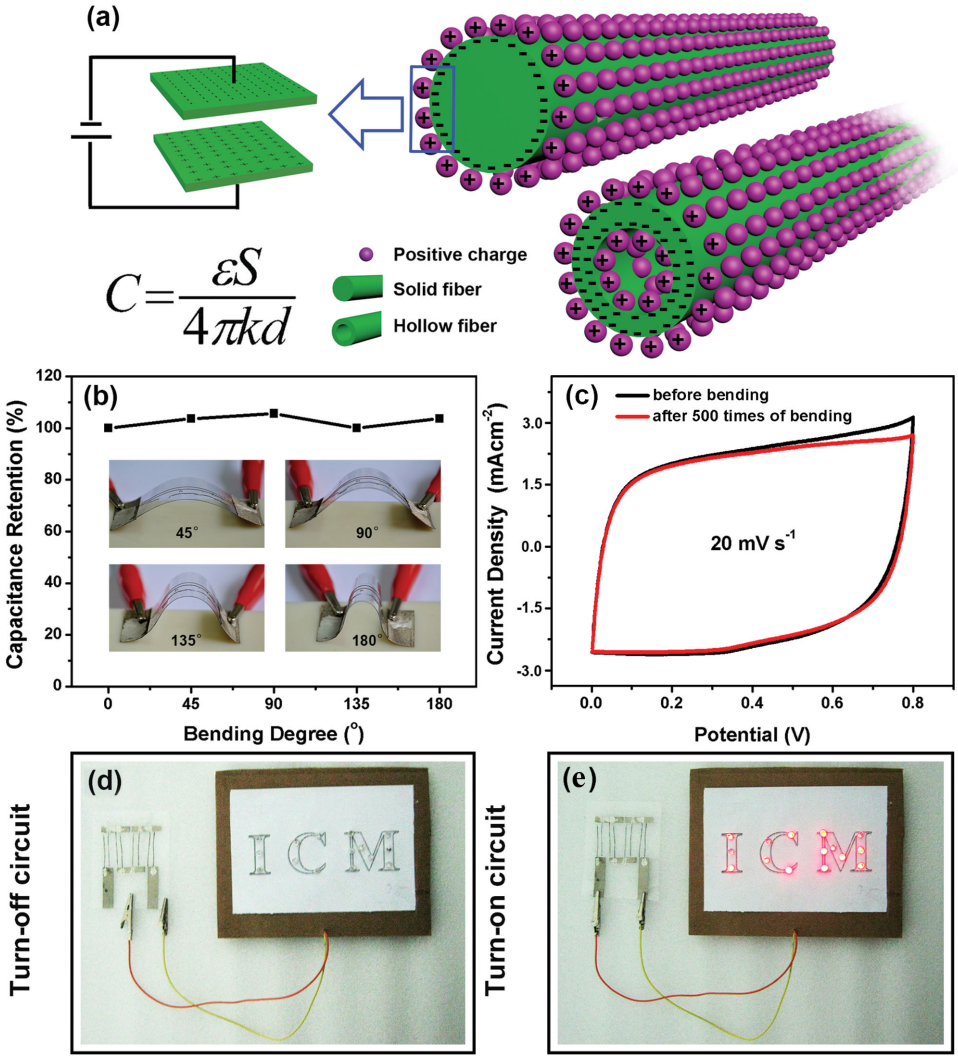

Figure 4. a) Schematic illustration to the charge distribution on the solid fiber, hollow fiber and parallel-plate capacitor. b) Capacitance retention under different bending states. c) CV curves of a flexible fiber supercapacitor before and after bending for 500 times. d,e) Photographs of four flexible, HCF-based supercapacitor fibers before and after connected to power 15 LEDs, respectively. The fiber supercapacitors share a length of 3.0 cm and are connected in series.

the significant contribution of the hollow structure to increase the specific capacitance.

The fiber-shaped supercapacitors were highly flexible and their electrochemical performances could be well maintained under various deformations (Figure 4b–e and Figure S4b (Supporting Information)), which is vital for their wearable applications. For instance, the specific capacitances remained almost unchanged under bending with increasing bending angles up to 180° (Figure 4b). In addition, the CV curves were almost overlapped before and after bending for 500 cycles (Figure 4c). The fiber-shaped supercapacitors could be readily connected in serial to provide a higher power output, e.g., four HCF-based supercapacitors were arranged to power 15 LEDs (Figure 4d,e). As expected, they could maintain high electrochemical performance even after bending to 180° (Figure S8, Supporting Information).

In summary, hollow fiber electrodes have been developed to fabricate novel and high-performance fiber-shaped supercapacitors. The fiber supercapacitors based on the hollow composite fiber reveal an ultra-high specific capacitance of 304.5 mF cm^{-2} (8.1 mF cm^{-1}, 143.3 F cm^{-3} or 63.1 F g^{-1}), which is 2–8 times of the other fiber-shaped supercapacitors. The energy densities based on the entire device and one fiber electrode reach 6.8 and 27.1 μW h cm^{-2}, respectively, which are also much higher than those of the previous reports. In addition, the high electrochemical performances are well maintained after cycling and bending. Considering the combined high mechanical and electrochemical properties, the fiber supercapacitors are particularly promising for the next-generation wearable electronics.

Supporting Information

Supporting Information is available from the Wiley Online Library or from the author.

© 2016 WILEY-VCH Verlag GmbH & Co. KGaA, Weinheim

Acknowledgements

This work was supported by the Applied Fundamental Foundation of Sichuan Province (2014JY0202), the R&D Foundation of China Academy of Engineering Physics (2014B0302036), the National Natural Science Foundation of China (21401177 and 21501160), the Science Foundation for Distinguished Young Scholars of Sichuan Province (2016JQ0025), the "1000plan" from the Chinese Government, the Collaborative Innovation Foundation of Sichuan University (XTCS2014009), and the Open Foundation of State Key Laboratory of Molecular Engineering of Polymers, Fudan University (K2013-19).

Received: February 3, 2016
Published online: March 22, 2016

[1] M. D. Lima, S. Fang, X. Lepró, C. Lewis, R. Ovalle-Robles, J. Carretero-González, E. Castillo-Martínez, M. E. Kozlov, J. Oh, N. Rawat, *Science* **2011**, *331*, 51.
[2] K. Cherenack, C. Zysset, T. Kinkeldei, N. Münzenrieder, G. Tröster, *Adv. Mater.* **2010**, *22*, 5178.
[3] M. Park, J. Im, M. Shin, Y. Min, J. Park, H. Cho, S. Park, M.-B. Shim, S. Jeon, D.-Y. Chung, *Nat. Nanotech.* **2012**, *7*, 803.
[4] L. Kou, T. Huang, B. Zheng, Y. Han, X. Zhao, K. Gopalsamy, H. Sun, C. Gao, *Nat. Commun.* **2014**, *5*, 3754.
[5] D. Yu, K. Goh, Q. Zhang, L. Wei, H. Wang, W. Jiang, Y. Chen, *Adv. Mater.* **2014**, *26*, 6790.
[6] J. Ren, L. Li, C. Chen, X. Chen, Z. Cai, L. Qiu, Y. Wang, X. Zhu, H. Peng, *Adv. Mater.* **2013**, *25*, 1155.
[7] Y. Hu, H. Cheng, F. Zhao, N. Chen, L. Jiang, Z. Feng, L. Qu, *Nanoscale* **2014**, *6*, 6448.
[8] K. Leitner, A. Lerf, M. Winter, J. Besenhard, S. Villar-Rodil, F. Suarez-Garcia, A. Martinez-Alonso, J. Tascon, *J. Power Sources* **2006**, *153*, 419.
[9] Z. Cai, L. Li, J. Ren, L. Qiu, H. Lin, H. Peng, *J. Mater. Chem. A* **2012**, *1*, 258.
[10] Q. Cheng, J. Tang, J. Ma, H. Zhang, N. Shinya, L.-C. Qin, *J. Phys. Chem. C* **2011**, *115*, 23584.
[11] R. Jalili, J. M. Razal, G. G. Wallace, *Sci. Rep.* **2013**, *3*, 3438.
[12] J. H. Park, J. M. Ko, O. O. Park, D.-W. Kim, *J. Power Sources* **2002**, *105*, 20.
[13] G. Sun, J. Liu, X. Zhang, X. Wang, H. Li, Y. Yu, W. Huang, H. Zhang, P. Chen, *Angew. Chem. Int. Ed.* **2014**, *126*, 12784.
[14] F. Su, M. Miao, *Nanotechnology* **2014**, *25*, 135401.
[15] K. Gopalsamy, Z. Xu, B. Zheng, T. Huang, L. Kou, X. Zhao, C. Gao, *Nanoscale* **2014**, *6*, 8595.
[16] K. Wang, Q. Meng, Y. Zhang, Z. Wei, M. Miao, *Adv. Mater.* **2013**, *25*, 1494.
[17] F. Su, X. Lv, M. Miao, *Small* **2015**, *11*, 854.
[18] E. Frackowiak, F. Beguin, *Carbon* **2001**, *39*, 937.
[19] V. T. Le, H. Kim, A. Ghosh, J. Kim, J. Chang, Q. A. Vu, D. T. Pham, J.-H. Lee, S.-W. Kim, Y. H. Lee, *ACS Nano* **2013**, *7*, 5940.
[20] Z. Xu, C. Gao, *Nat. Commun.* **2011**, *2*, 571.
[21] Q. Ji, X. Zhao, H. Liu, L. Guo, J. Qu, *ACS Appl. Mater. Interfaces* **2014**, *6*, 9496.
[22] T. Huang, B. Zheng, L. Kou, K. Gopalsamy, Z. Xu, C. Gao, Y. Meng, Z. Wei, *RSC Adv.* **2013**, *3*, 23957.
[23] M. Beidaghi, Y. Gogotsi, *Energy Environ. Sci.* **2014**, *7*, 867.
[24] D. Yu, Q. Qian, L. Wei, W. Jiang, K. Goh, J. Wei, J. Zhang, Y. Chen, *Chem. Soc. Rev.* **2015**, *44*, 647.
[25] Q. Wang, Z. Wen, J. Li, *Adv. Funct. Mater.* **2006**, *16*, 2141.
[26] Q. Meng, K. Wang, W. Guo, J. Fang, Z. Wei, X. She, *Small* **2014**, *10*, 3187.
[27] R. Liu, S. I. Cho, S. B. Lee, *Nanotechnology* **2008**, *19*, 215710.
[28] Z. Weng, Y. Su, D. W. Wang, F. Li, J. Du, H. M. Cheng, *Adv. Energy Mater.* **2011**, *1*, 917.
[29] Y. Ma, P. Li, J. W. Sedloff, X. Zhang, H. Zhang, J. Liu, *ACS Nano* **2015**, *9*, 1352.
[30] X. Dong, Z. Guo, Y. Song, M. Hou, J. Wang, Y. Wang, Y. Xia, *Adv. Funct. Mater.* **2014**, *24*, 3405.
[31] Z. Wang, D. O. Carlsson, P. Tammela, K. Hua, P. Zhang, L. Nyholm, M. Strømme, *ACS Nano* **2015**, *9*, 7563.
[32] J. Yan, Q. Wang, T. Wei, Z. Fan, *Adv. Energy Mater.* **2014**, *4*, 1300816.

© 2016 WILEY-VCH Verlag GmbH & Co. KGaA, Weinheim